ELSEVIER

Soil Dynamics and Earthquake Engineering 24 (2004) 877–886

SOIL DYNAMICS AND EARTHQUAKE ENGINEERING

www.elsevier.com/locate/soildyn

Multi-station analysis of surface wave dispersion

Chih-Ping Lin*, Tzong-Sheng Chang

Department of Civil Engineering, National Chiao Tung University, 1001 Ta-Hsueh Road, Hsinchu, Taiwan, ROC

Accepted 17 November 2003

Abstract

Methods based on multi-station recordings are presented for constructing the experimental dispersion curve of Rayleigh waves. Multi-station recording permits a single survey of a broad depth range, high levels of redundancy with a single field configuration, and the ability to adjust the offset, effectively reducing near field and far field effects. A method based on the linear regression of phase angles measured at multiple stations is introduced for determining data quality and filtering criteria. This method becomes a powerful tool for on site quality control in real time. The effects of multiple modes and survey line parameters, such as near offset, receiver spacing, and offset range, are investigated. Parametric studies result in general guidelines for the field data acquisition. A case study demonstrates how to easily deploy commonplace seismic refraction equipment to simultaneously record data for P-wave tomographic interpretation and multi-station analysis of surface wave.

Keywords: Surface wave; Shear-wave velocity

1. Introduction

The use of seismic methods to determine the underground stiffness is attractive since they are not affected by sample disturbance or insertion effects and are capable of sampling a representative volume of the ground even in difficult materials such as fractured rock or gravelly deposit. At shallow depths, surface seismic methods can determine stiffness-depth profiles without the need for boreholes that makes the subsurface seismic methods (such as down-hole and cross-hole methods) expensive and time consuming. Refraction survey is such a method that is widely used in geotechnical site investigation. Recent developments in refraction tomography have enhanced the spatial resolution of the refraction survey [1]. While P-wave refraction survey is quite effective, S-wave refraction survey may not provide the true S-wave velocity because of wave-type conversion in an area of non-horizontal layers [2]. Another type of surface seismic method makes use of surface waves. Surface-wave methods exploit the dispersion nature of Rayleigh waves. Measurements of phase velocity of Rayleigh waves of different frequencies (or wavelengths) can be used to determine a velocity-depth profile. The most common method used for obtaining the dispersion curve (a plot of phase velocity versus frequency or wavelength) is the spectral analysis of surface waves (SASW) [3–5].

In the current SASW practice, the dispersion curve is obtained using a two-receiver test configuration and the spectral analysis of the two signals. The SASW method gave a great contribution for the spreading of surface wave tests, but it also shows some drawbacks in field test and data analysis procedures that can be improved upon. It has been shown that errors may arise in experimental dispersion curves when usual SASW test and data analysis procedures are followed, in particular the phase unwrapping procedure. Sources that contain significant energy in very low frequencies and receivers with very low natural frequency are necessary to avoid erroneous un-wrapping of phase angles at low frequencies. Hence, the data acquisition system of a SASW test is typically different from that of a refraction survey although they share many things in common. Unwrapping errors may occur for sites where, across the frequency range used, there is a shift from one

* Corresponding author. Tel.: +886-3-513-1574; fax: +886-3-571-6257
E-mail address: cplin@mail.nctu.edu.tw (C.-P. Lin).

0267-7261/$ - see front matter © 2004 Elsevier Ltd. All rights reserved.
doi:10.1016/j.soildyn.2003.11.011

dominant surface wave propagation mode to another, a phenomenon termed 'mode jumping' [6]. Furthermore, the use of only a pair of receivers leads to the necessity of performing the test using several testing configuration and the so-called common receiver midpoint geometry. For each receiver spacing, multiple measurements are necessary for evaluating the data coherence. This results in a quite time-consuming procedure on site for the collection of all the necessary data and on data reduction for combining the dispersion data points from records obtained at all spacings. Since many non-trivial choices need to be made based on the data quality and testing configuration, the test requires the expertise of an operator and automation of the data reduction is difficult.

Other two-station methods using frequency-time analysis have been proposed to solve problems related to phase unwrapping and mode jumping [7,8]. However, the trade-off between the frequency and time resolution affects the result. Practical issues such as near field and attenuation also make the two-station methods difficult to apply. Methods based on multi-station data and f–k transform are recently reported to possess several advantages for surface wave analysis [9–11]. This paper thoroughly discusses methods of multi-station analysis of surface wave in different domains and their characteristics. A method using only the information of phase angles is introduced as an alternative or auxiliary method to the f–k transform. The effects of multiple modes and survey line parameters on the experimental dispersion curve are investigated in the context of multi-station analysis. This study also demonstrates how to easily deploy commonplace seismic refraction equipment to simultaneously determine the P- and S-wave velocity profiles using refraction tomography and multi-channel analysis of surface wave.

2. Spectral analysis of surface wave

2.1. Representation of surface waves

Neglecting material damping, the surface-wave signal u (be it displacement, velocity, or acceleration) for a single mode observed at a distance x from the source and a particular frequency $\omega(=2\pi f)$ is written as

$$u(x,t) = \frac{1}{\sqrt{x}} S(\omega) A(\omega) \mathrm{e}^{-\mathrm{j}\psi} \mathrm{e}^{-\mathrm{j}kx} \mathrm{e}^{\mathrm{j}\omega t} \tag{1}$$

where $S(\omega)$ is complex source spectrum, $A(\omega)\exp(-j\psi)$ represents the complex excitation of surface waves for a point source; k is the wave number whose reciprocal λ $(=2\pi/k)$ is the wavelength. The wave number is related to the phase velocity v by the definition $\omega = kv$. Eq. (1) represents the wave propagation and decay of a single-mode surface wave. The surface wave which includes multiple modes can be written as [12]

$$u(x,t) = \frac{1}{\sqrt{x}} S(\omega) \mathrm{e}^{\mathrm{jwt}} \sum_m A_m(\omega) \mathrm{e}^{-\mathrm{j}(k_m x + \psi_m)} \tag{2}$$

where the index m is the mode number. The presence of multiple modes complicates the interpretation of phase velocity. Eq. (2) can be written in the form of Eq. (1) as

$$u(x,t) = \frac{1}{\sqrt{x}} S(\omega) A'(\omega) \mathrm{e}^{-j\phi(x,\omega)} \mathrm{e}^{j\omega t} \tag{3}$$

where $A'(\omega)$ is the effective magnitude function of excitation and $\phi(x,\omega)$ is a composite phase function. The position of a given characteristic point of the harmonic wave (such for example a peak or a trough) is described by constant values of the phase:

$$\omega t - \phi(x,\omega) = \text{const} \tag{4}$$

Hence differentiating with respect to time, the local phase velocity $v(x)$ can be defined as

$$v(x) = \frac{\omega}{\frac{\partial \phi(x,\omega)}{\partial x}} \tag{5}$$

It is very important to note that since the Rayleigh wave velocity is a function not only of the frequency but also of the distance from the source, it is a local quantity.

2.2. Dispersion curves by spectral analysis of surface wave (SASW)

Surface waves in a typical SASW test are generated by an impact source, detected by a pair of geophones, and recorded on an appropriate recording device. The signals are recorded for several shots to evaluate the signal-to-noise ratio (or data coherence). The difference between the phase angles of the two signals $(\Delta\phi = \phi_2 - \phi_1)$ is equal to the phase angle of the average cross-spectral density $\mathrm{CSD}(u_1,u_2)$:

$$\Delta\phi(\omega) = \phi_2(\omega) - \phi_1(\omega) = \mathrm{Angle}[\mathrm{CSD}(u_1(t), u_2(t))] \tag{6}$$

Following Eq. (5), the apparent phase velocities of different frequencies can be determined as

$$v_\mathrm{a}(\omega) = \frac{\omega}{\frac{\Delta\phi(\omega)}{\Delta x}} \tag{7}$$

where Δx is the geophone spacing. The actual phase difference $\Delta\phi$ increases with frequency. But the angle of the cross-spectral density oscillates between $-\pi$ and π by definition. Thus, the angle of cross-power spectrum has to be un-wrapped before applying it to Eq. (7). This un-wrapping process is often a ticklish task. The correctness of un-wrapping at high frequencies relies on that at low frequencies. The energy generated by an impact source is band-limited, with low signal-to-noise ratio at very low and high frequencies. Geophones act as high-pass filters that damp the low-frequency components below the natural frequency of the geophones. Therefore, the signal-to-noise ratio of the signals is low below a particular frequency

depending on the source and receiver characteristics. Consequently, un-wrapping may be erroneous, especially for large geophone spacing since larger geophone spacing implies greater number of cycles in the phase spectrum. Removing of these un-wrapping errors is time consuming and depends on the analyst's judgment and experience. The natural frequency of geophones used for typical refraction survey is equal to or greater than 4.5 Hz, hence not suitable for SASW test. Wave Form Analyzer rather than typical seismograph is preferred because it has built-in spectral functions necessary for instantaneous inspection of the recorded data.

3. Multi-station analysis of surface wave

3.1. Multi-station spectral analysis of surface wave (MSASW)

The SASW method uses a minimum number of signals in space to determine the slope of $\phi(x)$ for Eq. (7) because multi-channel seismographs were not very common when the method was developed. The phase angles are un-wrapped in frequency domain. Errors in estimating the phase difference transform directly into errors in phase velocity calculation. Better estimation of dispersion curve can now be obtained based on a multi-station test configuration (Fig. 1), in which receivers are located at several locations along a straight line and a different data reduction scheme is used. Consider first a wavefield $u(t,x)$ of a single-mode surface wave with mode velocity $v=200$ m/s at a particular frequency $f=10$ Hz, as shown in Fig. 2. The wavefield is discretized and truncated in both the time and space domain during data acquisition. The sampling periods in the time and space domain are Δt and Δx; and the numbers of samples in the time and space domain are M and N, respectively. The single-frequency wavefield is obtained experimentally using a vibratory source or from the Fourier decomposition of a broadband transient wavefield incurred by an impact source. The spectral analysis of the multi-station signals can be performed using the discrete Fourier Transform [13]

$$U(f_i, x_n) = \frac{1}{M}\sum_{m=0}^{M-1} u(t_m, x_n)\exp(-\mathrm{j}2\pi f_i t_m) \tag{8}$$

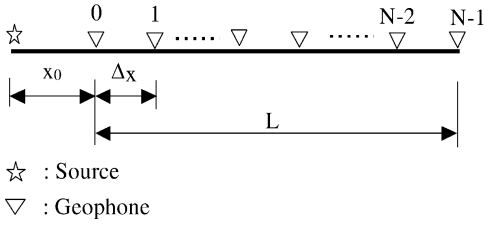

Fig. 1. A scheme of multi-station surface wave testing, in which x_0 is the near offset, Δx is the geophone spacing, and L is the offset range.

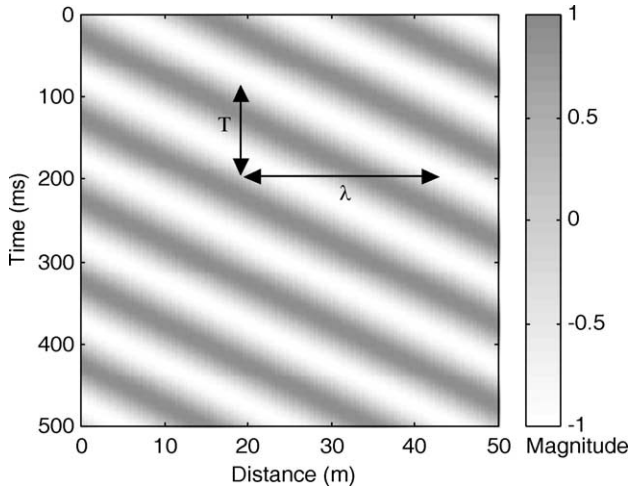

Fig. 2. An example wavefield of a single-mode surface wave ($f=10$ Hz, $v=200$ m/s in this case).

where $\mathrm{j}=\sqrt{-1}$, $t_m=m\Delta t$, $f_i=i\Delta f=i/[(M-1)\Delta t]$, and $x_n=n\Delta x$. The discretization and truncation in time domain may cause frequency aliasing and leakage in the spectral analysis [13]. The frequency aliasing can be avoided by using a sufficiently small Δt or the anti-aliasing filter in the data acquisition system such that

$$\Delta t < \frac{1}{2f_{\max}} \tag{9}$$

where $f_{\max}$ is the maximum attainable frequency of the signals. The leakage in the frequency domain does not occur when $(M-1)\Delta t$ is greater than the maximum duration of the transient signals incurred by an impact source. For stationary harmonic signals, the leakage in the frequency domain is lessened to an acceptable level by using a time window $(M-1)\Delta t$ greater than the maximum period of the signals or

$$(M-1)\Delta t > \frac{1}{f_{\min}} \tag{10}$$

where $f_{\min}$ is the lowest frequency of the vibratory source. The sampling interval and number of samples in most of modern data acquisition systems should be capable of avoiding problems related to frequency aliasing and leakage. The discrete Fourier transform is utilized for the spectral analysis because the Fast Fourier Transform (FFT) algorithm can be used for economically computing the transformations [13]. The frequency is also discretized in the discrete Fourier Transform. The frequency resolution is equal to $1/[(M-1)\Delta t]$.

The discrete Fourier transform of the wavefield $u(t_m,x_n)$ with respect to time (t_m) produces $U(f_i,x_n)$ with a modulo-2π representation in the phase spectrum. The phase angle can be un-wrapped in the space domain since it monotonically increases with the source-to-receiver offset x, as

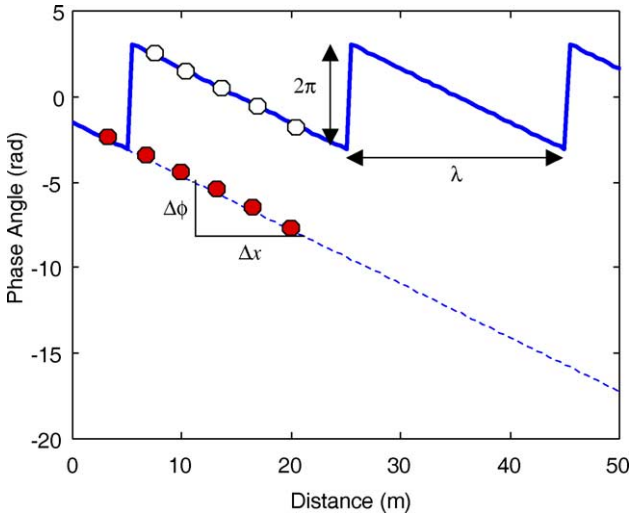

Fig. 3. An illustration of phase un-wrapping in the space domain for the multi-station spectral analysis of surface wave.

shown in Fig. 3. In order to correctly unwrapping the phase angles in the space domain, the following criterion should be satisfied

$$\Delta x < \frac{\lambda_{\min}}{2} \tag{11}$$

where $\lambda_{\min}$ is the shortest wavelength of interest. The phase velocity is clearly seen as the ratio of the wavelength (λ) to the period (T) in the wavefield (Fig. 2). It can be calculated numerically using Eq. (5). The slope of $\phi(x)$ is determined by the linear regression of the unwrapped $\phi(x_n)$, as shown in Fig. 3. The data quality can be evaluated by the R-square statistic (R^2) of the regression analysis. This method for determining the dispersion curve can be applied to both transient and stationary harmonic signals.

3.2. f–k analysis

Alternatively, the phase velocity may be determined by the f–k analysis [9]. For each frequency component, the wavefield is a harmonic function of space as can be inferred from Eq. (1) or (2). The wave number (i.e. spatial frequency) can be determined by a wave number analysis (spectral analysis in space). The wave number analysis of the multi-station signals can be performed using the discrete-space Fourier Transform [13]

$$Y(f_i,k) = \sum_{n=0}^{N-1} U(f_i,x_n)\exp(-\mathrm{j}kx_n) \tag{12}$$

Similarly, the discretization and truncation in the space domain may cause wave number aliasing and leakage. Wave number aliasing can be avoided by using a sufficiently small Δx as given by Eq. (11). According to the modal summation, $U(f_i,x_n)$ is a summation of harmonic functions in space. Analogous to Eq. (10), the measurement range in space (L) should be sufficiently long to avoid leakage error.

$$L = (N-1)\Delta x > \lambda_{\max} \tag{13}$$

where $\lambda_{\max}$ is the longest wavelength of interest. The discrete-space Fourier Transform is different from the discrete Fourier Transform in that the wave number remains continuous but the fast algorithm (FFT) cannot be used. The number of stations is typically much less than the number of samples in the time domain. So the discrete-space Fourier Transform rather than discrete Fourier Transform is used in the space domain to obtain a perfect wave number resolution. Fig. 4 shows the amplitude spectrum of the discrete-space Fourier transform of $U(f_i,x_n)$ with respect to space (x_n). The wave number (k) of the surface wave can be identified at the peak of the amplitude spectrum, as shown in Fig. 4. The phase velocity is determined by the definition $v = 2\pi f/k$.

The linear regression method (referred to as the MSASW method in this paper) is equivalent to the f–k transform method in theory but differs in practice. The MSASW method uses only the information of the phase and does not require constant geophone spacing. The geophone should be sufficiently small according to Eq. (11) to avoid aliasing that may cause errors in phase unwrapping. But the leakage is not an issue in MSASW analysis. Hence, a lone survey line given by Eq. (13) is not required. This is an important advantage for the MSASW method in practice. Furthermore, the data quality can be evaluated and filtering criteria may be determined using the $\phi(x_n)$ plot. The advantage of f–k transform method is that the phase-unwrapping procedure is completely avoided. These two methods are used collaboratively in practice. The two-station SASW method is very similar to the MSASW method in principle. But the MSASW method measures the phase angles at several offsets from the source, $\phi(x_n)$, rather than just the phase difference $\Delta\phi$ between two geophone locations.The linear regression attenuates the effect of

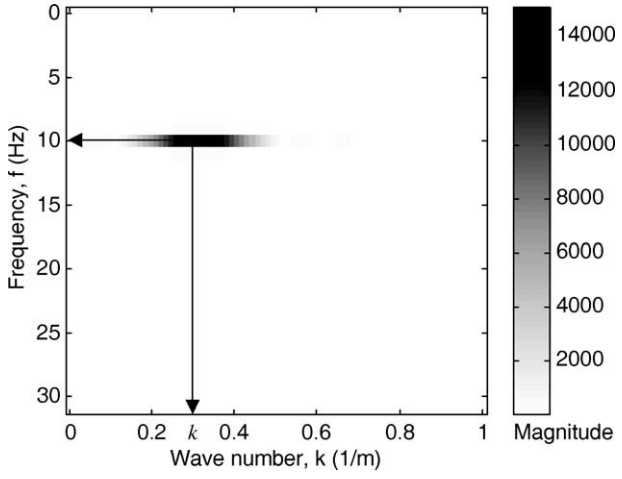

Fig. 4. Amplitude spectrum of the f–k analysis. The wave number of the surface wave is identified at the peak value.

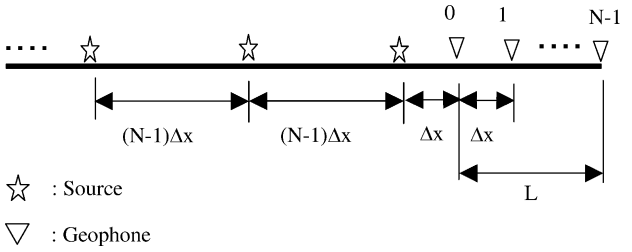

Fig. 5. A scheme of walk-away testing procedure.

possible phase-unwrapping errors because it's the slope that counts instead of the absolute value of phase difference. Moreover, un-wrapping in space domain has an advantage that poor data at very low frequencies can simply be discarded without affecting the results at higher frequencies. This is important for automating the construction of the dispersion curve.

4. Effects of higher modes

The number of available receivers limits the number of locations where the wavefield can be measured for a single shot. However, a wide range of source-to-receiver offsets can be covered by the walk-away test, as shown in Fig. 5, in which the source is moved away from the receivers to increase the near offset. The phase angle increases linearly with the source-to-receiver offset for a single mode of surface wave. However, when there are multiple modes, $\phi(x)$ becomes non-linear. Consider the wavefield of a single-frequency surface wave consisting of two modes as shown in Fig. 6. The mode velocities at $f=10$ Hz are $v_0=200$ m/s and $v_1=400$ m/s. Fig. 7 shows that $\phi(x)$ oscillates around the linear line of the dominant mode with an oscillation wavelength equal to $2\pi/\Delta k$, where $\Delta k=k_0-k_1$ is the difference between the wave numbers of the two modes.

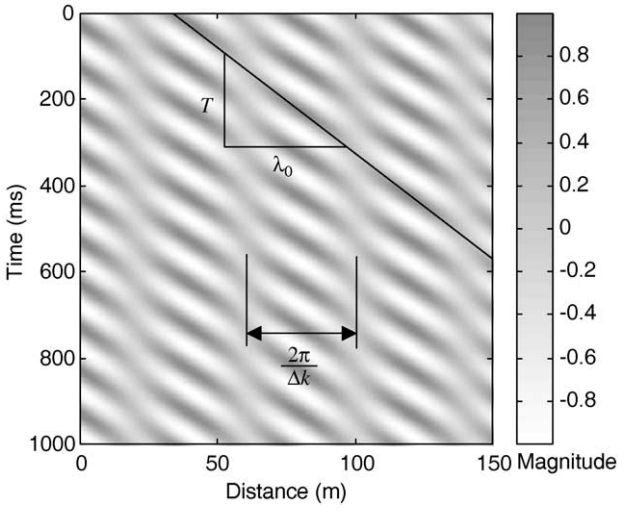

Fig. 6. An example wavefield of a multi-mode surface wave ($f=10$ Hz, $v_0=200$ m/s, and $v_1=400$ m/s in this case).

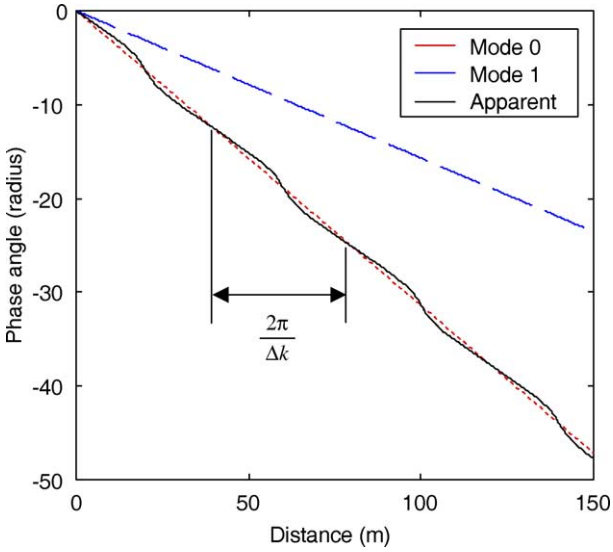

Fig. 7. Effects of multiple modes on the phase angle as a function of the source-to-receiver offset. The phase velocities at 10 Hz for Mode 0 and Mode 1 are 200 and 400 m/s, respectively. The amplitude ratio of Mode 0 to Mode 1 is 6:4.

The linear regression of the data $\phi(x_n)$ represents $\phi(x)$ of the dominant mode if the total length of the survey line is long enough. Fig. 8 shows the residuals of the regression analysis, $\Delta\phi(x)$, the difference between the measured $\phi(x)$ and the regressed line. It is possible to determine Δk from this plot. The velocity or wave number of the second mode can then be determined as well. However, f–k transform method is more effective in mode separation, especially when more than two modes are present. Fig. 9 shows the amplitude spectrum of the f–k transform with two peaks indicating two different modes. Lower peaks in the amplitude spectrum may also be resulted from the leakage due to truncation of the infinite wavefield. The residual plot ($\Delta\phi$ vs. x) can assist in determining whether the peak is due to the multiple modes or leakage. The ability to separate two modes depends on the length of the survey line (L) and how close adjacent two modes are. The criteria for mode separation can be written as

$$L \gg \frac{2\pi}{\Delta k} \tag{14}$$

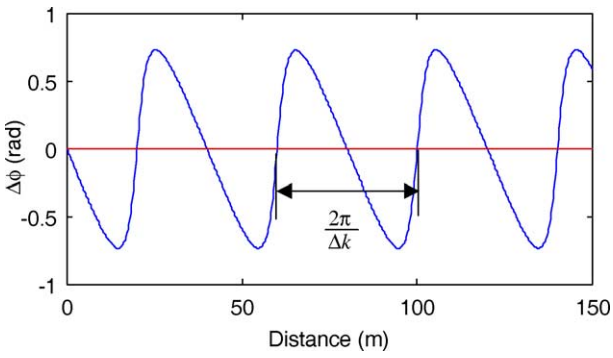

Fig. 8. The residual plot of the regression analysis of $\phi(x_n)$.

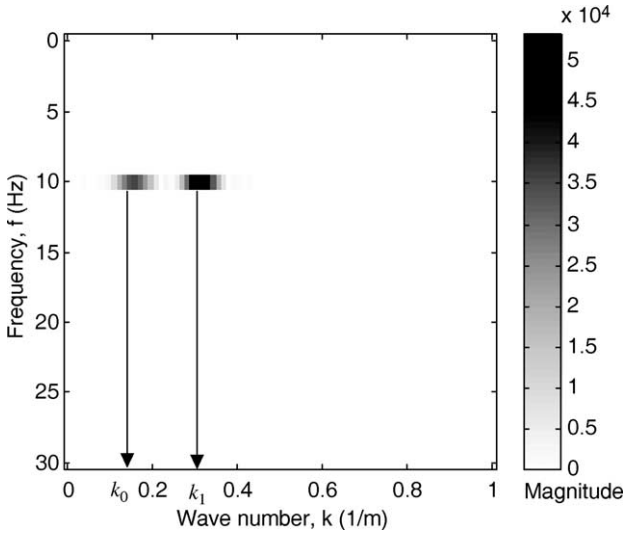

Fig. 9. *f–k* Amplitude spectrum of the multi-mode wavefield. The wave numbers of multiple modes are identified at the peak values.

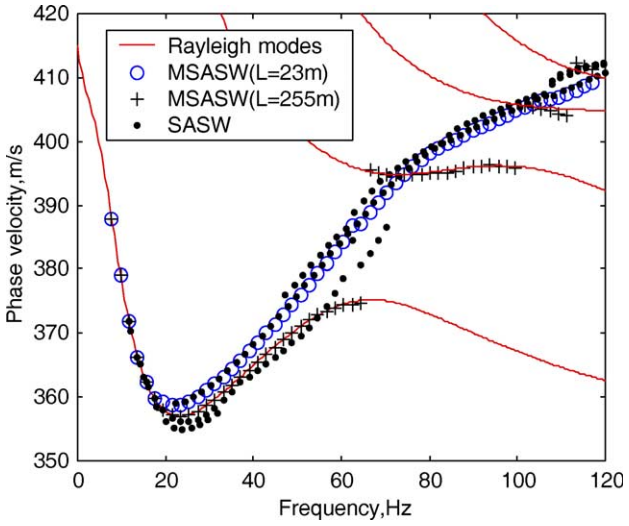

Fig. 10. Effect of offset range on the measured dispersion curve ($x_0 = 1$ m; $\Delta x = 1$ m).

The peaks associated with two adjacent modes in the *f–k* amplitude spectrum cannot be distinguished if the above criterion is not satisfied. The single peak in the *f–k* amplitude spectrum corresponds to the apparent velocity resulted from the two modes. This apparent phase velocity is equivalent to that obtained by the linear regression of $\phi(x_n)$.

For a normally dispersive profile in which the fundamental mode dominates, $\phi(x)$ is a good linear function for each frequency and the apparent phase velocity coincides with the fundamental mode. The experimental dispersion curve can be inverted for the shear wave velocity profile by considering only the fundamental mode. However, a higher mode or multiple modes dominate in some frequency range, especially for deposits with V_s varying irregularly with depth [14]. Fig. 7 conceptually illustrates the effect of modal superposition on the apparent phase velocity. It is desirable to further investigate the effect of higher modes in the context of an inversely dispersive profile and MSASW analysis.

Consider a shear wave velocity profile of regular stratification overlaid by a harder surface layer, as shown in Table 1, same as that considered by Foti [11]. Higher modes dominate in some frequency ranges in such a case. Synthetic seismograms are generated using the modal summation of surface waves [15] for source-to-receiver offsets from 1 to 256 m on a 1 m interval. The sampling period of the synthetic seismograms is 0.002 s and the number of data points is 1024. Body waves (near field effects) are not considered in the modal summation to simplify the study of the effect of multiple modes. The synthetic data was analyzed by the MSASW method. Fig. 10 shows the apparent dispersion curves for a small offset range ($L = 23$ m) and a large offset range ($L = 255$ m). Also shown in Fig. 10 are the Rayleigh modes. When the offset range is large enough, the resulting dispersion curve becomes piecewise continuous curve with sudden mode jumpings when different modes dominate at different frequencies. In cases where L is not long enough to obtain $\phi'(x)$ of the dominant mode, the resulting smooth curve represents the apparent dispersion curve of the test configuration, which typically has a smooth transition between modes. The dispersion curves obtained from the absolute maximum peaks in the *f–k* amplitude spectra are the same as that obtained by the MSASW method. In addition, participating modes can be identified using the *f–k* analysis when Eq. (14) is satisfied. In practice, the offset range is restricted by the available space, near field effect and attenuation. And it is not known a priori if L is long enough to separate individual modes. Current practice in the inversion process utilizes only the fundamental mode. The model compatibility between the experimental and theoretical dispersion curve has to be considered in cases where the apparent dispersion curves do not coincide with the fundamental mode.

Table 1
A system with a harder surface layer

Thickness (m)	V_s (m/s)	V_p (m/s)	Density (kg/m^3)
3	450	800	1800
5	350	600	1800
10	400	700	1800
∞	450	800	1800

The synthetic data was also analyzed using the SASW method. The SASW test was simulated including the following geophone spacings: 1, 2, 4, 8, 16, 32, 64, 128 m. The usual filtering criterion ($\lambda/3 <$ geophone spacing $< 2\lambda$) was applied to the constructed dispersion curves [3]. The experimental dispersion curves obtained by the SASW method are also shown in Fig. 10. The dispersion curve segments obtained for different geophone spacings follow the trend of the apparent dispersion curve obtained by first 24-channel MSASW. The scatter of the SASW data in this synthetic case is due solely to multiple modes.

Different geophone spacings in a SASW test may produce quite different phase velocities at the same frequency even after the filtering process. It should be noted that Eq. (7) is a measure of the apparent phase velocity. The dispersion curve of the predominant mode is obtained only if one mode dominates. The filter criteria do not ensure the condition that the measured wavefield is predominated by one mode; it only mitigates the effects of near field and far field. The wide scatter of the data in the field may be attributed to multiple modes as much as to the noise. Combining the scattered data produced by different geophone spacings in a SASW test is an extra work that may result in extra uncertainty.

The fact that the apparent phase velocity is defined by the receiver locations relative to the source has to be emphasized in the case of multiple modes. Fig. 11 shows the effect of near offset (x_0) on the apparent dispersion curves for a small offset range ($L=23$ m). The dispersion curve obtained for $x_0=1$ m differs slightly from that for $x_0=20$ m. No one is better than the other, if near field and attenuation effects are not considerer. They are different simply because the apparent velocity is a local quantity. The linear regression of $\phi(x_n)$ depends on the spatial position where it is evaluated. The frequency resolution Δf is equal to 0.4883 in Fig. 10. The results are shown for every $4\Delta f$. To obtain phase velocities at frequencies of integer number, only the first 1000 points of the seismic records were used so that Δf is equal to 0.5 Hz in Fig. 11. The circles in Figs. 10 and 11 represent the same multi-station testing configuration. The results are slightly different at frequencies around 60 and 100 Hz. These regions correspond to mode jumping and frequencies of low energy in the synthetic data. Also shown in Fig. 11 are the results of the SASW analysis for $\Delta f=0.5$ Hz. The segments of dispersion curves are more scattered in this case. The results for geophone spacing 2 and 4 m even fall out of the plotting range. The SASW method is more sensitive to noise and mode jumping, especially in the phase un-wrapping procedure. Un-wrapping the phase angles in the space domain is more robust than un-wrapping in the frequency domain. The apparent phase velocities obtained by *f–k* analysis are the same as that obtained by MSASW analysis except for $L=23$ m and frequencies below 5 Hz, in which Eq. (13) is not satisfied (i.e. the wavelength is longer than offset range).

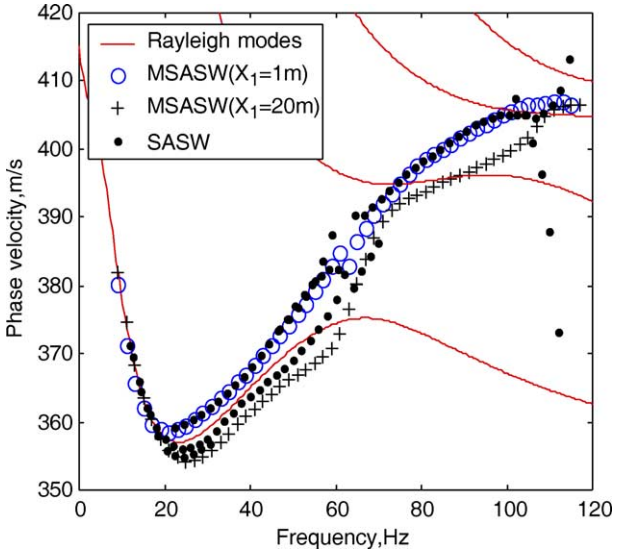

Fig. 11. Effect of near offset on the measured dispersion curve ($\Delta x=1$ m; $L=23$ m).

5. Experimental study

5.1. Effects of source-to-receiver offsets

Eqs. (9)–(14) provide the theoretical guidelines for selecting proper data acquisition parameters in a field test including temporal parameters, Δt and M, and spatial parameters, Δx and N. In practice, the available testing space, source characteristics, near field effect, and attenuation restrict the range of source-to-receiver offsets where $\phi(x)$ can be measured accurately for a particular frequency. Hence, the apparent velocity in a MSASW test is determined from the average slope of $\phi(x)$ over some source-to-receiver offsets, where $\phi(x_n)$ varies smoothly with x_n. The selection of the proper offset range is analogous to the filtering criteria in the SASW test. However, the filtering process in the SASW test is applied to the constructed dispersion curve, in which the high-frequency values may have already been contaminated by the poor data at low frequencies due to near field effect or low signal-to-noise ratio at low frequencies. The filtering process in the MSASW method is prior to the construction of the dispersion curve.

To avoid spatial aliasing, geophone spacing (Δx) should not be greater than half the shortest wavelength, which is approximately equal to the minimum definable thickness. The MSASW method does not require a long survey line for normally dispersive profiles. Although a long survey line is desirable to identify individual modes in Rayleigh waves when multiple modes participate, it is often impractical and it is not known a priori how long is long enough. A short survey line may be acceptable for multi-mode surface waves if the location-dependent apparent dispersion curve is taken into consideration in the inversion process. Therefore, it is possible to obtain the dispersion curve for the desired frequency range with a single test configuration. Experiments were conducted at a test site to investigate the effect of near offset (x_0) on multi-station measurements. Twenty-four geophones were deployed on a 1 m interval with the near offset ranging from 10 to 30 m. The seismograph is a 24-channel OYO model McSeis-SX. The geophones are OYO Geospace model GS-11D vertical velocity transducer, having a natural resonant frequency of 4.5 Hz. A 6 kg sledgehammer was used as the impact source.

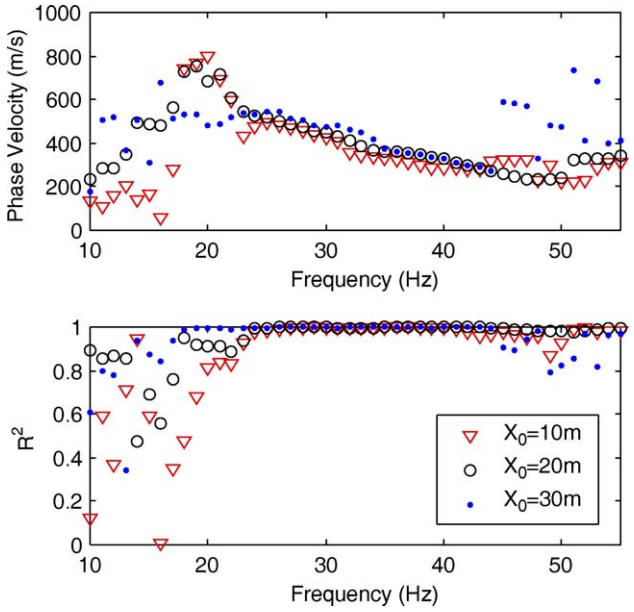

Fig. 12. Experimental dispersion curves and R^2 values obtained for different near offsets ($\Delta x = 1$ m and $L = 23$ m).

Fig. 12 shows the measured dispersion curve and R^2 for near offset 10, 20, and 30 m. A higher mode dominates at frequencies greater than 50 Hz as shown in Fig. 12 for $x_0 =$ 10 m. The interference of higher modes at frequencies above 50 Hz is confirmed by the f–k analysis. Because of undesirable near-field effects, Rayleigh waves can only be treated as horizontally traveling plane waves after they have propagated a certain distance from the source point [16]. Plane-wave propagation of surface wave does not occur in most cases until the near offset (x_0) is greater than at least half the maximum desired wavelength. Acceptable data extends to lower frequencies as near offset increases as expected, as shown in Fig. 12. However, there is a mitigation of near field effects on the dispersion curve estimation by the linear regression of multi-station data. The measurable frequency also decreases as near offset increases. Although it is generally true that surface wave is much more energetic than body waves, the high-frequency (short-wavelength) components lose their energy quite rapidly because they normally propagate through the shallowest veneer of the surface where attenuation is most significant. Contamination by body waves because of attenuation of high-frequency ground roll at longer offsets is referred to as the far field effect [10]. This effect limits the highest frequency at which phase velocity can be determined.

Near field and far field effects affect the measurable frequency range for each test configuration (Fig. 1). If a greater range of frequency is of interest, a wide range of offsets can be obtained by a walk-away test. And the optimum offset range for each frequency can be selected from the plot of $\phi(x_n)$. This filtering process improves the data accuracy and further extends the measurable frequency range. However, different locations of the geophones used to determine the phase velocity for each frequency should be taken into account in the case of multiple modes. The source characteristic, background noises, and geological conditions also play important roles in the measurable frequency range. The MSASW analysis can be performed in real time on site for quality control. Results like Fig. 12 can be obtained instantaneously after the data acquisition. Necessary adjustments to the testing procedure can then be made.

5.2. MSASW interpretation of refraction data

The same type of geophones used for body-wave surveying can be used for MSASW tests. The field configuration of a MSASW test is similar to that for body-wave surveying with only a slightly different criterion for selecting the optimum field configuration and acquisition parameters. In many cases the surface wave analysis can be performed coincident with or as a by-product of the body-wave surveying. An example is presented herein to show how to analyze the same refraction surveying data with P-wave refraction tomography and MSASW method to simultaneously estimate the P- and S-wave velocity profiles. A P-wave refraction survey was conducted in a project involving the investigation of a fault near the Science and Technology Park in Hsinchu, Taiwan. The same equipment described above was used in this project. Twenty-four geophones were deployed on a 5 m interval. Seven shots were generated to obtain wide ray coverage for the tomography analysis with five shots inside the survey line and two end shots outside the survey line. During the classical refraction tests using impact sources, the recording time was increased in order to detect Rayleigh waves. The traveltime tomography analysis using the commercial software SeisOpt®Pro™ Version 1.0 utilized all data from the seven shots. The resulting P-wave tomogram justifies the assumption of horizontal layering of the subsurface for

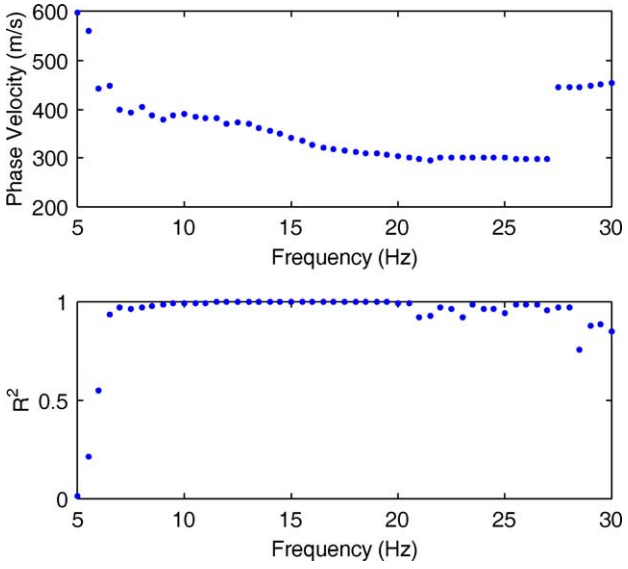

Fig. 13. Experimental dispersion curve and R^2 values obtained by MSASW analysis of a refraction surveying data.

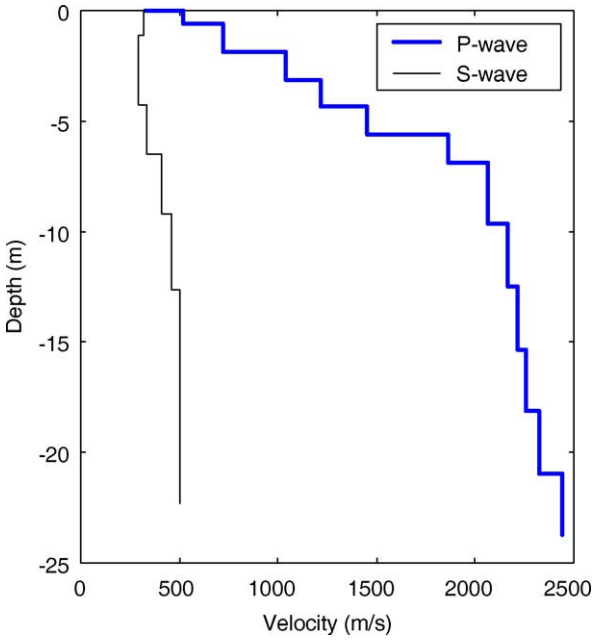

Fig. 14. The S- and P-wave velocity profiles of the refraction test site.

the surface wave analysis. The data generated by the shot near the first geophone was used for surface wave analysis. Fig. 13 presents the experimental dispersion curve and R^2 of the linear regression. A higher mode dominates at frequencies above 27 Hz. The part of experimental dispersion curve between 7 and 27 Hz is identified as the fundamental mode and used for data inversion. A non-linear inversion was performed with the method developed by Xia et al. [17]. The velocity profile obtained from the refraction tomography analysis provides P-wave velocity values needed in the inversion process. The resulting shear wave and compression wave velocity profiles are shown in Fig. 14. This example demonstrates how one can effectively estimate P- and S-wave velocities simultaneously from a single seismic survey using traveltime tomography and MSASW technique.

6. Conclusions

This study is aimed at discussing the multi-station analysis of surface wave to recommend a better procedure to construct the experimental dispersion curve including data acquisition, test configuration, and data analysis. The multi-station spectral analysis of surface wave (MSASW) and *f–k* transform method utilize commonplace seismic refraction equipment for data acquisition and a test configuration similar to body-wave surveying. The multi-station methods resolve the difficulties encountered in the traditional SASW test. The MSASW method is based on the linear regression of phase angles measured at multiple stations, in which data quality can be evaluated and filtering criteria can be determined. It is a power tool for on site quality control in real time. When used together with *f–k* transform, MSASW selects the proper range of offsets for constructing the dispersion curve and assist in multiple mode identification.

The effects of multiple modes on multi-station measurements are investigated and the criterion of mode separability is discovered. The offset range required to separate two modes is inversely proportional to the difference in wave number. The experimental dispersion curve represents the location-dependent apparent dispersion curve for multi-mode surface waves when the survey line is not long enough. The modal compatibility between the experimental and theoretical dispersion curve needs to be considered in the inversion process. In practice, the available testing space, source characteristics, near field effect, and attenuation restrict the range of source-to-receiver offsets where the phase angles can be measured accurately for each frequency. A walk-away test plus the filtering process gives the best coverage of frequencies. The multi-station recordings mitigate the near field effect. It is often possible to obtain the dispersion curve for the desired frequency range with a single test configuration. A case study demonstrates how to analyze classical refraction data with P-wave refraction tomography and MSASW method to simultaneously estimate the P- and S-wave velocity profiles.

Acknowledgements

Funding for this research was provided by the National Science Council of ROC under contracts No. 89-2218-E-009-104 and 90-2611-E-009-009.

References

[1] Pullammanappallil SK, Louie JN. A generalized simulated-annealing optimization for inversion of first arrival times. Bull Seismol Soc Am 1994;84(5):1397–409.
[2] Xia J, Miller RD, Park CB. A pitfall in shallow shear-wave refraction surveying SEG, 69th Annual Meeting, Houston, TX 1999 p. 508–11.
[3] Heisey JS, Stokoe II KH, Hudson WR, Meyer AH. Determination of in situ shear wave velocities from spectral analysis of surface waves. Research Report No. 256-2, Center for Transportation Research, The University of Texas at Austin; 1982. p. 277.
[4] Nazarian S, Stokoe II KH. In situ shear wave velocities from spectral analysis of surface waves Proceedings of Eighth Conference on Earthquake Engineering, San Francisco, vol. 3 1984 p. 38–45.
[5] Stokoe II KH, Wright GW, James AB, Jose MR. Characterization of geotechnical sites by SASW method. In: Woods RD, editor. Geophysical characterization of sites. Rotterdam: A.A. Balkema; 1994, p. 15–25.
[6] Al-Hunaid MO. Difficulties with phase spectrum unwrapping in SASW nondestructive testing of pavements. Can Geotechn J 1992;29: 506–11.
[7] Al-Hunaidi MO. Analysis of dispersed multi-mode signals of the SASW method using multiple filter/cross correlation technique. Soil Dyn Earthq Engng 1994;13:13–24.

[8] Karray M, Lefebvre G. Identification and isolation of multiple modes in Rayleigh waves testing methods Geotechnical Special Publication No. 108.: ASCE; 2000 p. 80–94.
[9] Gabriels P, Snieder R, Nolet G. In situ measurements of shear-wave velocity in sediments with higher-mode Rayleigh waves. Geophys Prospect 1987;35:187–96.
[10] Park CB, Miller RD, Xia J. Multichannel analysis of surface waves. Geophysics 1999;64(3):800–8.
[11] Foti S. Multistation methods for geotechnical characterization using surface waves. Politecnico di Torino. PhD Dissertation; 2000.
[12] Aki K, Richards PG. Quantitative seismology, theory and method—2 vol. San Francisco: Freeman; 1980.
[13] Prokis JG, Manolakis DG. Digital signal processing—principles, algorithms, and applications, 3rd ed. New Jersey: Prentice Hall; 1992.
[14] Tokimatsu K, Tamura S, Kojima H. Effects of multiple modes on Rayleigh wave dispersion characteristics. J Geotech Engng 1992; 118(10):1529–43.
[15] Herrmann RB. Computer programs in seismology. Ver. 3.20. Saint Louis University, Missouri; 2002.
[16] Richart FE, Hall JR, Woods RD. Vibrations of soils and foundations. New Jersey: Prentice Hall; 1970.
[17] Xia J, Miller RD, Park CB. Estimation of near-surface shear-wave velocity by inversion of Rayleigh waves. Geophysics 1999;64:691–700.